Inorganic Chemistry

Article

pubs.acs.org/IC

Overoxidation of Phenol by Hexachloroiridate(IV)

Na Song and David M. Stanbury*

Department of Chemistry and Biochemistry, Auburn University, Auburn, Alabama 36849, United States

Supporting Information

ABSTRACT: It has been previously established that the aqueous oxidation of phenol by a deficiency of $[IrCl_6]^{2-}$ proceeds through the production of $[IrCl_6]^{3-}$ and phenoxyl radicals. Coupling of the phenoxyl radicals leads primarily to 4,4′-biphenol, 2,2′-biphenol, 2,4′-biphenol, and 4-phenoxyphenol. Overoxidation occurs through the further oxidation of these coupling products, leading to a rather complex mixture of final products. The rate laws for oxidation of the four coupling products by $[IrCl_6]^{2-}$ have the same form as those for the oxidation of phenol itself: $-d[Ir^{IV}]/dt = \{(k_{ArOH} + k_{ArO^-}K_a/[H^+])/(1 + K_a/[H^+])\}[ArOH]_{tot}[Ir^{IV}]$. Values for k_{ArOH} and k_{ArO^-} have been determined for the four substrates at 25 °C and are assigned to H_2O-PCET and electron-transfer mechanisms, respectively. Kinetic simulations of a combined mechanism that includes the rate of oxidation of phenol as well as the rates of these overoxidation steps show that the degree of overoxidation is rather limited at high pH but quite extensive at low pH. This pH-dependent overoxidation leads to a pH-dependent stoichiometric factor in the rate law for oxidation of phenol and causes some minor deviations in the rate law for oxidation of phenol. Empirically, these minor deviations can be accommodated by the introduction of a third term in the rate law that includes a "pH-dependent rate constant", but this approach masks the mechanistic origins of the effect.

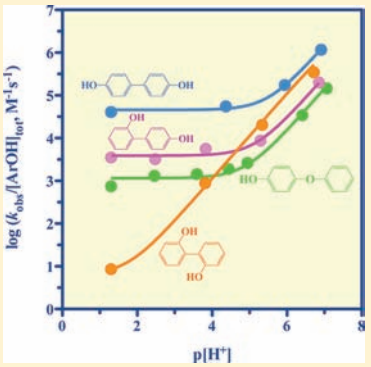

INTRODUCTION

Redox reactions in aqueous solution are often accompanied by changes in protonation. When the reactions proceed via one-electron steps, the phenomenon of proton-coupled electron transfer (PCET) is often involved. The breadth of importance of PCET is immense, and PCET is of great significance because it is often an absolute criterion of reactivity.[1] One approach to gaining insight into PCET is to study reactions in which one of the reactants is a typical inorganic outer-sphere electron-transfer reagent with no acid/base properties: this constraint confines much of the electron-proton coupling considerations to the other reaction partner. The oxidation of phenols has become central in developing the concepts of PCET, in part because of its importance in revealing the function of tyrosine in redox proteins but also because these reactions are quite amenable to study. Accordingly, the oxidation of phenol by $[IrCl_6]^{2-}$ has been the focus of a classic publication,[2] and it is now of interest as a model for reactions where electron transfer occurs in concert with proton transfer to the solvent: H_2O-PCET.[3−5]

Despite its importance, the oxidation of phenol by $[IrCl_6]^{2-}$ presents certain difficulties. One of these is that the phenolic products are a complex mixture,[2] and it is unclear how the post-rate-limiting steps lead to this mixture. It is also unclear whether these latter stages in the reaction have any influence on the measurements of the putative rate-limiting steps. Of further concern is the pH dependence of the rates, which displays deviations from the classic two-term rate law for such reactions[5] and might provide additional evidence in support of a pH-dependent rate constant, as has been reported previously for the oxidation of phenol by $[Ru(bpy)_3]^{3+}$.[6] Herein is reported a study of the $[IrCl_6]^{2-}$ oxidations of the four major products derived from coupling of the phenoxyl radical. These rates are then incorporated into an overall mechanism for the oxidation of phenol, which shows that overoxidation is responsible for many of the reaction products. Moreover, it is shown that the degree of overoxidation is pH-dependent and that this can account for the observed deviations from the classical two-term rate law.

EXPERIMENTAL SECTION

Reagents and Solutions. All commercial chemical reagents were used as received except as noted. Ammonium hexachloroiridate(III) monohydrate (Ir^{III}), 2,6-dimethylacetanilide, chlorosulfonic acid, 3-chloroperoxybenzoic acid, *N*-*tert*-butylphenylnitrone (PBN), α-(4-pyridyl-*N*-oxide)-*N*-*tert*-butylnitrone (POBN), 2-methyl-2-nitrosopropane (MNP), 5,5-dimethyl-1-pyrroline *N*-oxide (DMPO), deuterium oxide, 3,5-dibromosulfanilic acid sodium salt, 2-iodophenol, 4-hydroxyphenyl boronic acid, palladium(II) acetate, 1,1′-bis-(diphenylphosphino)ferrocence (dppf), potassium carbonate, sodium acetate anhydrous, cacodylic acid, and sodium hydroxide were purchased from Sigma-Aldrich Chemical Co. Perchloric acid, ammonium perchlorate, sodium chloride, ammonium chloride, copper(II) nitrate trihydrate, acetic acid, monochloroacetic acid, ethanol, diethyl ether, 1,4-dioxane, petroleum ether, ethyl acetate, acetonitrile, hydrochloric acid, and hydrogen peroxide were from Fisher Scientific Co. 2,2′-Biphenol, 4,4′-biphenol, and 4-phenoxyphenol were commercially available from Acros Organics. Ammonium hexachloroiridate(IV) (Ir^{IV}) was purchased from Alfa or prepared according to the literature[7] by the addition of ammonium chloride (Fisher) to a solution of sodium hexachloroiridate(IV) hexahydrate. Phenol (Fluka) was recrystallized from a 75% (w/w) water solution as in the literature.[8]

Received: August 30, 2011
Published: November 16, 2011

All solutions were freshly prepared with deionized water provided by a Barnstead NANO Pure Infinity ultrapure water system and purged with argon gas prior to reaction to prevent potential complications caused by O_2. In order to increase the concentration of the solution, 4,4′-biphenol or 2,4′-biphenol was first dissolved in CH_3CN or ethanol and then diluted with water to make a reaction solution where less than 1% (w/w) organic solvent was present. The ionic strength was adjusted by lithium perchlorate trihydrate (GFS) and was approximately equal in both solutions to prevent Schlieren effects. Selected buffer solutions (acetate, monochloroacetate, and cacodylate buffers) were applied to control the pH if necessary.

Preparation of Sodium 3,5-Dibromo-4-nitrosobenzenesulfonate (DBNBS). This compound was synthesized from 3,5-dibromosulfanilic acid sodium salt according to the method of Kaur et al.[9] and further purified using procedure type C of Hamilton et al.[10] A mixture of 3,5-dibromosulfanilic acid (10 mmol), anhydrous sodium acetate (10 mmol), 7.9 mL of a 30% aqueous hydrogen peroxide solution, and 30 mL of glacial acetic acid was warmed gently to dissolve the solid. The solution was stored at room temperature for 14 days. Then the crude yellow solid product was collected and washed with glacial acetic acid, cold ethanol, diethyl ether/1,4-dioxane (1:1), and cold ethanol again. A pale-yellow powder was obtained after drying. Yield: 30%. Mp: >300 °C. ^{1}H NMR (D_2O): δ 8.30 (s, 2H). ^{13}C NMR (D_2O): δ 119.10 (aryl CBr), 131.03 (aryl CH), 141.00 (aryl CSO_3Na), 147.61 (aryl CNO).

Preparation of Sodium 2,4-Dimethyl-4-nitrosobenzenesulfonate (DMNBS). This compound was prepared according to the literature.[11,12] 2,6-Dimethylacetanilide (18 mmol) was added into 10 mL of cold $ClSO_3H$ with stirring. After reacting for 15 min at 5 °C, 1 h at 25 °C, and 10 min at 40 °C, the mixture was poured onto cracked ice to form a white solid of the sulfonyl chloride. Then this compound was treated with concentrated HCl under reflux for 1 h before neutralization by NaOH to produce sodium 2,6-dimethylaniline-3-sulfonate. The sodium sulfonate (10 mmol) was dissolved in 30 mL of methanol and oxidized by *m*-chloroperoxybenzoic acid (10 mmol) with stirring for 1 h at room temperature. Then ether was added to precipitate the final product. Yield: 80%. ^{1}H NMR (D_2O): δ 2.56 (s, 3H), 2.75 (s, 3H), 7.54 (d, 1H), 8.13 (d, 1H).

Preparation of 2,4′-Biphenol. 2,4′-Biphenol was prepared through a Pd-catalyzed Suzuki–Miyaura coupling reaction according to the literature.[13] Under dry nitrogen, 4-hydroxyphenyl boronic acid (1.4 mmol), $Pd(OAc)_2$ (0.14 mmol), bis(diphenylphosphino)-ferrocene (dppf) (0.14 mmol), and K_2CO_3 (3 mmol) were added to a solution of 2-iodophenol (1 mmol) in 10 mL of tetrahydrofuran. The reaction was stirred under reflux for 1 day and monitored by thin-layer chromatography. After the reaction completed, the crude product was purified by column chromatography on silica gel (eluent PE/EtOAc = 3.5/1). Then, sublimation was performed under vacuum at 160 °C to remove the nonvolatile metal residue impurities, and resublimation was carried out at 110 °C to remove the volatile impurities. Yield: 50%. Mp: 161.2–162.8 °C. ^{1}H NMR ($CDCl_3$; Figure S-1 in the Supporting Information): δ 4.89 (s, 1H), 5.14 (s, 1H), 6.94–6.99 (m, 4H), 7.20–7.24 (m, 2H), 7.34–7.36 (m, 2H).

Methods. A Corning 450 pH/ion meter was used with a Mettler Toledo InLab 421 or InLab Semi-Micro-L combination pH electrode. The reference electrode electrolyte was replaced with 3 M NaCl to prevent the formation of $KClO_4$ precipitate. Electrode calibrations at μ = 0.1 M ($LiClO_4$) were carried out with 0.01–0.1 M perchloric acid. With the known H^+ concentration and pH reading, the activity coefficient γ (=0.839 ± 0.04) was obtained from the equation $p[H^+] = pH + \log \gamma$, where $p[H^+]$ is equal to $-\log [H^+]$. When the pK_a of 4,4′/2,4′-biphenol is measured, an alkaline error may occur with pH values higher than 11. Thus, we calibrated the electrode with 1×10^{-3} M NaOH at μ = 0.1 M ($LiClO_4$) and found that the true pH is equal to the apparent pH plus 0.3.

All measurements were performed at 25.0 ± 0.1 °C. The kinetic experiments were carried out on a Hi-Tech SF-51 stopped-flow spectrophotometer with OLIS 4300 data acquisition and analysis software. UV–vis spectra were monitored on a HP-8453 diode-array spectrophotometer equipped with a Brinkman Lauda RM6 thermostatted water bath to maintain the temperature at 25 °C. Because $(NH_4)_2[IrCl_6]$ has strong absorbance around 488 nm while the corresponding product $(NH_4)_3[IrCl_6]$ does not, as shown in Figure S-2 (Supporting Information), all kinetic data were obtained by monitoring the absorbance of Ir^{IV} at λ_{max} (488 nm) with ε_{488} = (3.9 ± 0.1) × 10^3 M^{-1} cm^{-1}.[14] In order to detect the DBNBS influence on the reactions of phenol, we also observed the absorbance change over the wavelength 400–525 nm at intervals of 25 nm. For the phenol and 4-phenoxyphenol reactions, the observed pseudo-first-order rate constants were obtained from the fitting of kinetic traces over 5 half-lives to first-order exponential functions. For 4,4′-biphenol and 2,2′-biphenol, the observed initial rate constants were determined from the slope of the linear regression of the logarithm of absorbance at 488 nm within the first half-life, while for 2,4′-biphenol, the rate constants were obtained from double-exponential fits. Each reported observed rate constant is the average of at least five shots. The *Specfit/32*, version 3.0.15, global analysis system was applied to simulate the reaction traces, and the *GraphPad Prism 4 or 5* software was used to analyze the rate law with $1/Y^2$ weighting.

^{1}H and ^{13}C NMR spectra were acquired on a Bruker AV 400 MHz spectrometer; chemical shifts in $CDCl_3$ are relative to tetramethylsilane, and those in D_2O are relative to DSS. The melting points were obtained using an Electrothermal IA 9100 digital melting point apparatus. Cyclic voltammograms (CV) and Osteryoung square-wave voltammograms were performed on a BAS 100B electrochemical analyzer equipped with a BAS C3 cell stand and a purging and stirring system; a glassy carbon electrode was the working electrode, Ag/AgCl (3.0 M NaCl) was the reference electrode ($E°$ = 0.205 V vs NHE),[15] and a Pt wire was the auxiliary electrode.

Quantum calculations of the electronic spectra were performed with the *Spartan '08* software package.[16]

RESULTS

Results for the oxidation of phenol by Ir^{IV} have already appeared in preliminary form.[5] Results for oxidation of the four coupling products are shown here for the first time.

The kinetic traces for the consumption of 1×10^{-4} M Ir^{IV} in its reaction with a large excess of phenol were obtained at various $p[H^+]$ at 488 nm, the absorbance maximum of Ir^{IV}. Figure 1a exhibits a typical kinetic trace for a reaction with 0.44 M phenol in 0.05 M $HClO_4$ ($p[H^+]$ = 1.3). Such kinetic traces do not give good fits with either first- or second-order rate laws. As the $p[H^+]$ increases, good-quality pseudo-first-order fits are obtained at both $p[H^+]$ = 2.9 and 4.8 with 0.044 M phenol (Figure 1b,c). At high $p[H^+]$ (=7.1), the reaction with 1.8×10^{-3} M phenol is much faster and becomes non-pseudo-first-order again (Figure 1d). These results show a strong $p[H^+]$ effect on phenol oxidation by Ir^{IV}. As shown below, the deviations at low pH arise from inhibition by Ir^{III}, while the deviations at high pH are due to the absorbance of phenolic products.

Kinetic Inhibition by Ir^{III}. At $p[H^+]$ = 1.3, Figure 2a shows the effects of adding a 5-fold excess of Ir^{III} under conditions otherwise identical with those in Figure 1a. The retarding effect of Ir^{III} at this pH is seen to be quite strong and clearly can be expected to cause deviations from pseudo-first-order kinetics of the type shown in Figure 1a. On the other hand, at $p[H^+]$ = 7.1, no Ir^{III} inhibition is observed with the addition of 5- and 10-fold excess of Ir^{III} (Figure 2b,c), and so the deviations from pseudo-first-order kinetics at this pH (Figure 1d) are due to factors other than inhibition by Ir^{III}.

Basicity of Ir^{III}. The basicity of Ir^{III} was probed by measuring the pH dependency of the cyclic voltammetry of 1×10^{-3} M Ir^{IV} in the $p[H^+]$ range 0–2 at 1 M ionic strength ($LiClO_4$). $p[H^+]$ values were adjusted by $HClO_4$ according to $p[H^+] = -\log [HClO_4]$. Reversible CVs ($E_{1/2}$ = 0.717 ± 0.007 V vs Ag/AgCl) were obtained over this pH range. No pH dependence of $E_{1/2}$ was observed under all of these conditions, which implies that

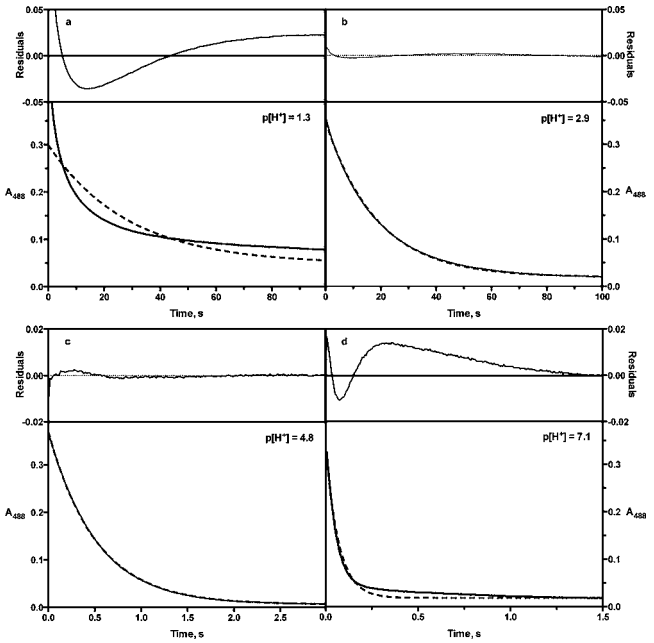

Figure 1. Kinetic traces of the oxidation of phenol by 1×10^{-4} M Ir^{IV} at different p[H^+] values. The lower boxes show the experimental traces (solid lines) and the pseudo-first-order fits (dashed lines). The upper boxes show the residuals in the fits. μ = 0.1 M ($LiClO_4$); T = 25 °C. (a) $[phenol]_{tot}$ = 0.44 M; $[HClO_4]$ = 0.05 M. (b) $[phenol]_{tot}$ = 0.044 M; p[H^+] = 2.9 (0.02 M monochloroacetate buffer). (c) $[phenol]_{tot}$ = 0.044 M; p[H^+] = 4.8 (0.02 M acetate buffer). (d) $[phenol]_{tot} = 1.8 \times 10^{-3}$ M; p[H^+] = 7.1 (0.02 M cacodylate buffer).

Ir^{III} is not significantly basic even in 1 M H^+. Bruhn et al. observed a small but significant dependence of $E_{1/2}$ over this same pH range in H^+/Na^+ media;[17] we attribute this effect to the differing specific interaction coefficients of these two ions.

General Base Catalysis Tests. Tests for general base catalysis of the reaction of phenol with Ir^{IV} were described previously.[5] In brief, they show that the reaction is not catalyzed by low concentrations of the cacodylate buffer at pH 6.5, by low concentrations of ammonia at pH 7, or by low concentrations of phenoxide at pH 5.1. These results show that the kinetic data presented herein on phenol oxidation by Ir^{IV} are free of complications arising from general base catalysis. This conclusion is in agreement with the recent report from Irebo et al. and Bonin et al. that general base catalysis in outer-sphere phenol oxidation can be insignificant under certain conditions.[4,18,19]

Spin Trapping. Several conventional spin traps (illustrated in Scheme 1) were investigated for their effects on the kinetics of the phenol/Ir^{IV} reaction in 0.05 M H^+. As we have reported previously, DBNBS is quite effective in this regard.[5] Figure 3 illustrates the dramatically improved fit to a first-order rate law achieved with only 10 mM DBNBS. The other spin traps PBN, DMPO, POBN, and MNP barely affect the reaction, and DMNBS is only partially effective (Table S-1 in the Supporting Information). These results are not unexpected, given the known specificity of DBNBS for phenoxyl radicals.[20] Tests in 0.05 M H^+ with concentrations of DBNBS ranging from 0.1 to 15 mM (Table S-2 in the Supporting Information) show that the effects saturate at about 5 mM DBNBS. A standard DBNBS concentration of 10 mM is used in the experiments described below. The approach to saturation is expected to be dependent on both the efficiency of phenoxyl radical scavenging and the DBNBS dimerization equilibrium (K = 1.3×10^{-3} M).[21]

Scheme 1. Structure of Spin-Trapping Agents Tested

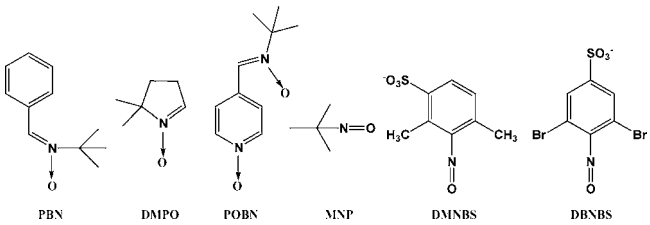

The effects of DBNBS are also significant at p[H^+] = 7. The results (Table S-3 in the Supporting Information) show that DBNBS removes the deviations from pseudo-first-order kinetics that are otherwise seen at this pH. The effect is attributed to DBNBS interception of phenoxyl radicals, the dimerization of which would lead to absorbing intermediates (biphenoquinones), as shown below.

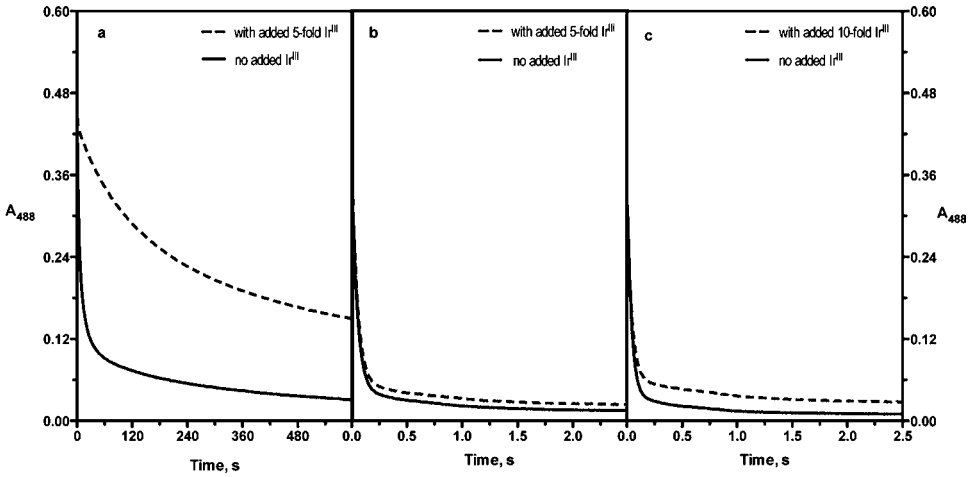

Figure 2. Comparative traces of the phenol reaction with added Ir^{III} (dashed line) and no added Ir^{III} (solid line). $[Ir^{IV}]_0 = 1 \times 10^{-4}$ M; μ = 0.1 M ($LiClO_4$); T = 25 °C. (a) $[phenol]_{tot}$ = 0.44 M; $[Ir^{III}] = 5 \times 10^{-4}$ M; $[HClO_4]$ = 0.05 M. (b) $[phenol]_{tot} = 1.8 \times 10^{-3}$ M; $[Ir^{III}] = 5 \times 10^{-4}$ M; p[H^+] = 7.1 (0.02 M cacodylate buffer). (c) $[phenol]_{tot} = 1.8 \times 10^{-3}$ M; $[Ir^{III}] = 1 \times 10^{-3}$ M; p[H^+] = 7.1 (0.02 M cacodylate buffer).

dx.doi.org/10.1021/ic201897m | Inorg. Chem. 2011, 50, 12762–12773

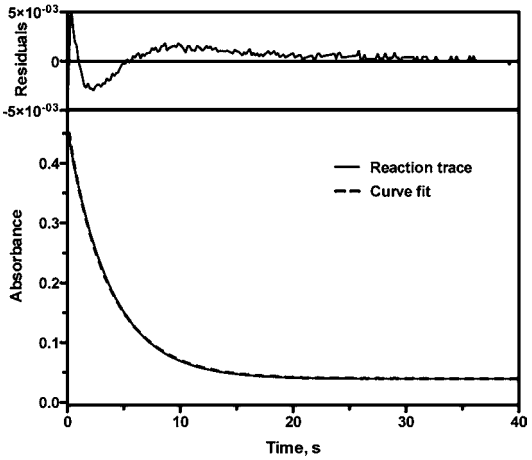

Figure 3. Trace of the phenol reaction with added DBNBS. The lower box shows the experimental trace (solid line) and the pseudo-first-order fit (dashed line). The upper box shows the residuals in the fit. $[\text{phenol}]_{tot}$ = 0.44 M; $[Ir^{IV}]_0 = 1 \times 10^{-4}$ M; [DBNBS] = 10 mM; $[HClO_4]$ = 0.05 M; μ = 0.1 M ($LiClO_4$); T = 25 °C.

Phenol Dependence. In results already published, it was shown that the rate of oxidation of phenol by Ir^{IV} is first-order in [phenol].[5] This result was obtained in 0.05 M $HClO_4$ with 10 mM DBNBS and also at p[H^+] = 5.1 without DBNBS. The conditional rate constants are 0.612 ± 0.001 at p[H^+] = 1.3 and 106 ± 4 at p[H^+] = 5.1, and they indicate that the kinetics are sensitive to p[H^+].

p[H^+] Dependence. A simple two-term rate law arises from the assumption that both phenol and the phenolate anion can react with Ir^{IV}, as shown by eqs 1 and 2.

$$-\frac{d[Ir^{IV}]}{dt} = \frac{k_{ArOH} + k_{ArO^-}K_a/[H^+]}{1 + K_a/[H^+]}[ArOH]_{tot}[Ir^{IV}] \quad (1)$$

$$\frac{k_{obs}}{[ArOH]_{tot}} = \frac{k_{ArOH} + k_{ArO^-}K_a/[H^+]}{1 + K_a/[H^+]} = \frac{k_{ArOH} + k_{ArO^-} \times 10^{p[H^+]-pK_a}}{1 + 10^{p[H^+]-pK_a}} \quad (2)$$

Here, K_a is the acid dissociation constant of phenol, $pK_{a,ArOH}$ = 9.79 at μ = 0.1 M.[22] k_{ArOH} and k_{ArO^-} represent the reactivities of phenol and the phenolate anion.

Between p[H^+] = 2.4 and 6.8, the oxidation of phenol by Ir^{IV} yields good-quality pseudo-first-order fits, as shown in Figures 1b,c. This feature enables us to study the p[H^+] effect on the rate constants from p[H^+] = 2.46 to 6.74 with 1×10^{-4} M Ir^{IV} and $(4.43–44.3) \times 10^{-3}$ M phenol. Selected buffers were employed to maintain the p[H^+] values. The data are summarized in Table S-4 in the Supporting Information, and a plot of $k_{obs}/[\text{phenol}]_{tot}$ versus p[H^+] is shown in Figure 4. A nonlinear least-squares fit of the data to eq 2 shows that the rates conform to this two-term rate law with k_{ArOH} = 0.54 ± 0.02 M^{-1} s^{-1} and $k_{ArO^-} = (5.0 \pm 0.1) \times 10^6$ M^{-1} s^{-1}.

As described above, in the presence of 10 mM DBNBS, the kinetic traces obey pseudo-first-order kinetics over the wider p[H^+] range of 1–7. Experiments above pH = 7 were not performed because of the known instability of Ir^{IV} at high pH.[23] The details of these experiments have been published,[5] and they show that the reaction obeys eq 2 with rate constants about 50% greater than those without the addition of DBNBS:

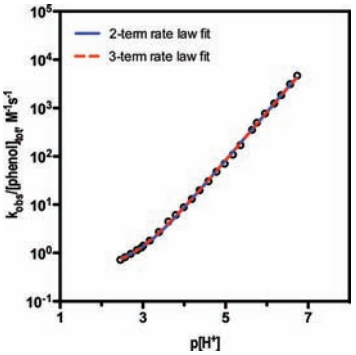

Figure 4. Plot of $k_{obs}/[\text{phenol}]_{tot}$ versus p[H^+] in the absence of DBNBS. $[Ir^{IV}]_0 = 1 \times 10^{-4}$ M; μ = 0.1 M ($LiClO_4$); T = 25 °C. The p[H^+] values between 2.4 and 3.4 were maintained by a 0.02 M monochloroacetate buffer; the p[H^+] values between 3.6 and 5.4 were maintained by a 0.02 M acetate buffer; the p[H^+] values between 5.6 and 7.0 were maintained by a 0.02 M cacodylate buffer. The solid line is the fit to eq 2, and the dashed line is the fit to eq 3. Data are from Table S-4 in the Supporting Information.

k_{ArOH} = 0.77 ± 0.03 M^{-1} s^{-1} and $k_{ArO^-} = (8.0 \pm 0.2) \times 10^6$ M^{-1} s^{-1}. As discussed below, this rate increase induced by DBNBS is attributed to differing stoichiometric factors.

Inclusion of the *k*° Term. It has been reported that eq 2 is inadequate to describe the reaction of phenol with $[Ru(bpy)_3]^{3+}$, and a "pH-dependent rate constant" (the $k°$ term) was introduced as in eq 3 to fit the data.[6]

$$\frac{k_{obs}}{[ArOH]_{tot}} = \frac{k_{ArOH} + k° \times 10^{0.5p[H^+]} + k_{ArO^-} \times 10^{p[H^+]-pK_a}}{1 + 10^{p[H^+]-pK_a}} \quad (3)$$

When the pH-dependent data for oxidation by Ir^{IV} with no added DBNBS are fit with eq 3, the optimized values are k_{ArOH} = 0.40 ± 0.06 M^{-1} s^{-1}, $k_{ArO^-} = (4.9 \pm 0.1) \times 10^6$ M^{-1}, and $k° = (6.5 \pm 3) \times 10^{-3}$ M^{-1} s^{-1} (Table S-5 in the Supporting Information). This fit yields slightly improved residuals, but the values of k_{ArOH} and k_{ArO^-} are virtually unchanged. Over the p[H^+] range 1–7, the maximum contribution of the $k°$ term to the total rate is 16% and occurs around p[H^+] = 2.7. Although this $k°$ term has only marginal statistical significance, we show below that it is a consequence of pH-dependent stoichiometric factors.

As we reported previously,[5] in the presence of DBNBS, fitting the data to eq 3 yields slightly improved residuals relative to eq 2 (Table S-6 in the Supporting Information). The fitted values for k_{ArOH} and k_{ArO^-} are only slightly changed: k_{ArOH} = 0.59 ± 0.03 M^{-1} s^{-1}, $k_{ArO^-} = (7.3 \pm 0.1) \times 10^6$ M^{-1}, and $k° = (2.0 \pm 0.3) \times 10^{-2}$ M^{-1} s^{-1}. The maximum contribution from the $k°$ term is 28% and appears at the same p[H^+] as that in the result without DBNBS. The origin of the $k°$ term in the presence of DBNBS is currently unknown but is speculated to arise from a pH-dependent overoxidation of the DBNBS/phenoxyl adduct.

Kinetic Isotope Effect (KIE). We have previously reported on the deuterium KIE in the reaction between phenol and Ir^{IV}.[5] It was measured by comparing the rates in a D_2O solution to those in normal H_2O. The experiments were performed at $[H^+]$ = 0.09 M in the presence of 10 mM DBNBS, and thus the KIE refers to k_{ArOH}. The rates are independent of the pH under these conditions, so the equilibrium isotope effect on K_a is not an issue. The KIE value is 3.5 ± 0.3, which clearly indicates a

dx.doi.org/10.1021/ic201897m | Inorg. Chem. 2011, 50, 12762–12773

primary KIE and implies cleavage of the O−H bond in the rate-limiting step. Although this result is taken as evidence of a concerted PCET mechanism (see below), the measured KIE is not extremely large, so it is conceivable that the measured k_{ArOH} value includes a small contribution from a parallel sequential PCET mechanism. Focusing on the (major) concerted PCET component, the solvent (water) must be acting as the proton acceptor because Ir^{III} is not appreciably basic and no other bases appear in the rate law. A similar KIE and mechanism were recently reported for the oxidation of phenol by three $Ru^{III}(bpy)_3$-type complexes[3] and for the oxidation of hydroxylamine by Ir^{IV}.[24]

Coupling Products. As we described in our previous communication,[5] the second step in the reaction between phenol and Ir^{IV} is the self-reaction of the phenoxyl radicals. This self-reaction is currently believed to occur through C−C and C−O coupling to generate the four major expected product isomers in Scheme 2. According to pulse radiolysis

Scheme 2. Expected Dimerization Products of the Phenoxy Radical and Their Composition According to Reference 25

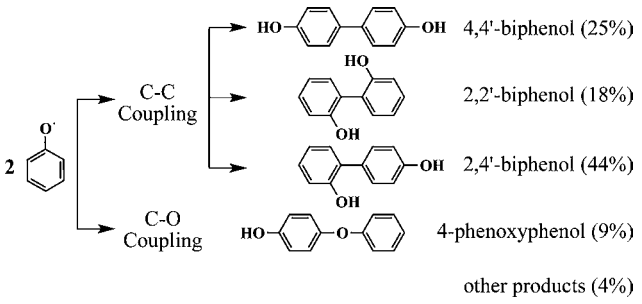

experiments,[25] the yields of these products are 25% for 4,4′-biphenol, 18% for 2,2′-biphenol, 44% for 2,4′-biphenol, and 9% for 4-phenoxyphenol. The remaining 4% is other products.

The UV−vis spectra of the four coupling isomers in H_2O or a 0.2% ethanol/water mixture are shown in Figure 5. 4,4′-Biphenol

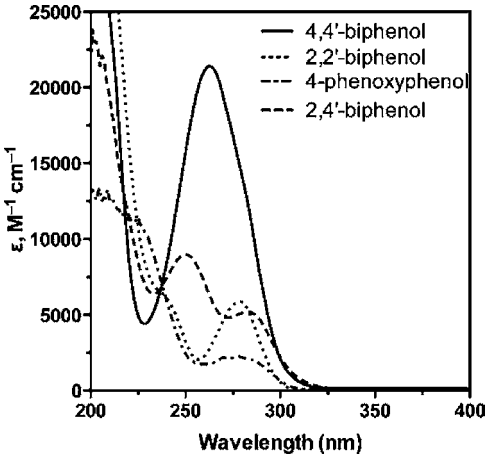

Figure 5. UV−vis spectra of 4,4′-/2,2′-/2,4′-biphenol and 4-phenoxyphenol in water or a 0.2% ethanol/water solution.

has strong absorption at 263 nm with a molar absorptivity (ε_{263}) of 2.1×10^4 M^{-1} cm^{-1}. The maximum absorption wavelength is red-shifted to 279 nm when the structure changes to 2,2′-biphenol, and its ε_{279} value is 5.9×10^3 M^{-1} cm^{-1}. Two absorption bands are observed for 2,4′-biphenol: 250 and 283 nm ($\varepsilon_{250} = 9.0 \times 10^3$ M^{-1} cm^{-1} and $\varepsilon_{283} = 5.2 \times 10^3$ M^{-1} cm^{-1}). The spectrum of 4-phenoxyphenol exhibits a weaker and broader absorption at 278 nm with $\varepsilon_{278} = 2.2 \times 10^3$ M^{-1} cm^{-1}.

pK_a Values of 4,4′-Biphenol and 2,4′-Biphenol. Spectrophotometric titration with NaOH was used to determine the two pK_a values for 4,4′-biphenol because controversial results were found previously.[26−28] At 0.1 M ionic strength ($LiClO_4$), 3×10^{-5} M 4,4′-biphenol was titrated from pH = 6.5 to 12.6 with various amounts of NaOH, generating the series of UV−vis spectra shown in Figure S-3 in the Supporting Information. These spectra show a loss of absorbance at 260 nm due to consumption of biphenol and a gain of absorbance at 288 nm. The titration curve at 288 nm, after volume correction, is sigmoidal, as shown in Figure 6. Satisfactory fits of this curve to

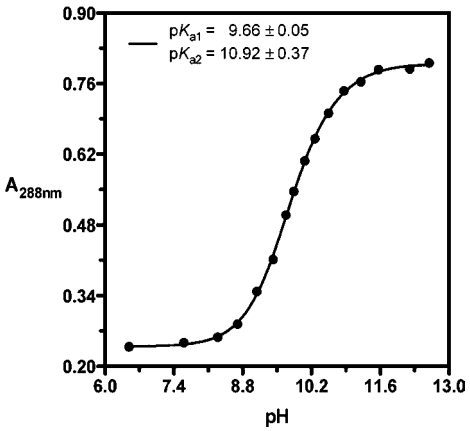

Figure 6. Titration curve of 4,4′-biphenol at 288 nm after volume correction. μ = 0.1 M ($LiClO_4$); T = 25 °C. The solid line is the fit to eq 4.

a model involving a single ionizable proton could not be obtained. On the other hand, an excellent fit was obtained with a model that included two ionizable protons, as in eq 4.

$$A = \frac{\varepsilon_{HOArArO^-}c}{1 + 10^{pH-pK_{a2}} + 10^{pK_{a1}-pH}} + \frac{\varepsilon_{OArArO^-}c}{1 + 10^{pK_{a2}-pH} + 10^{pK_{a1}+pK_{a2}-2pH}} + \frac{\varepsilon_{HOArArOH}c}{1 + 10^{pH-pK_{a1}} + 10^{2pH-pK_{a1}-pK_{a2}}} \quad (4)$$

Equation 4 expresses the total absorbance (A) as a function of the pH, pK_{a1}, and pK_{a2}, the total biphenol concentration (c), and the molar absorptivities (ε) for all three protonated and deprotonated forms. The result of the fit to eq 4 is shown in Figure 6, and the derived values are $pK_{a1} = 9.66 \pm 0.05$ and $pK_{a2} = 10.92 \pm 0.4$, $\varepsilon_{HOArArO^-} = 2.4 \times 10^4$ M^{-1} cm^{-1}, $\varepsilon_{-OArArO^-} = 2.7 \times 10^4$ M^{-1} cm^{-1}, and $\varepsilon_{HOArArOH} = 8.0 \times 10^3$ M^{-1} cm^{-1}. The pK_{a1} value is very close to that reported by Jonsson et al.,[27] and the pK_{a2} value is as expected for successive pK_a values.

A similar titration of 2,4′-biphenol led to the complex series of spectra shown in Figure S-4 in the Supporting Information. The titration curve at 310 nm (Figure 7) is sigmoidal, but the curve at 285 nm clearly shows that three species are involved. A fit of the absorbance data at 285 nm to eq 4 yields the following values: $pK_{a1} = 9.65 \pm 0.04$, $pK_{a2} = 10.96 \pm 0.06$, $\varepsilon_{HOArArO^-} = 8.5 \times 10^3$ M^{-1} cm^{-1}, $\varepsilon_{-OArArO^-} = 6.1 \times 10^3$ M^{-1} cm^{-1}, and $\varepsilon_{HOArArOH} = 5.2 \times 10^3$ M^{-1} cm^{-1}. A fit at 310 nm yields $pK_{a1} = 9.68 \pm 0.04$, $pK_{a2} = 10.89 \pm 0.05$, $\varepsilon_{HOArArO^-} = 4.8 \times 10^3$ M^{-1} cm^{-1},

dx.doi.org/10.1021/ic201897m | Inorg. Chem. 2011, 50, 12762–12773

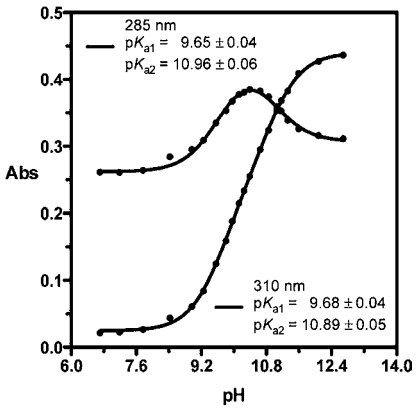

Figure 7. Titration curves of 2,4′-biphenol at 285 and 310 nm after volume correction. μ = 0.1 M ($LiClO_4$); T = 25 °C. The solid lines are the fits to eq 4.

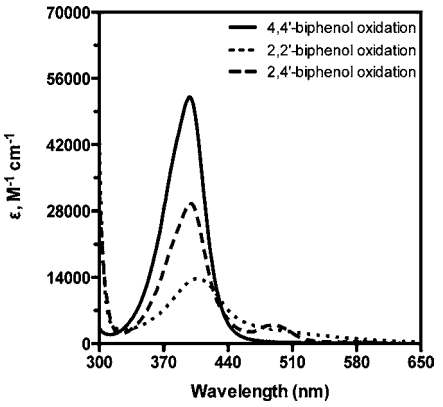

Figure 8. UV−vis spectra of products of 4,4′-/2,2′-/2,4′-biphenol oxidation. $[Ir^{IV}]_0 = 2.5 \times 10^{-5}$ M; μ = 0.1 M ($LiClO_4$); T = 25 °C. The solid line is 4,4′-biphenol oxidation: $[4,4'\text{-biphenol}]_0 = 2.5 \times 10^{-5}$ M; $p[H^+]$ = 5.5 (0.02 M acetate buffer). The short dashed line is 2,2′-biphenol oxidation: $[2,2'\text{-biphenol}]_0 = 1 \times 10^{-3}$ M; $p[H^+]$ = 4.0 (0.02 M acetate buffer). The long dashed line is the 2,4′-biphenol reaction: $[2,4'\text{-biphenol}]_0 = 2 \times 10^{-4}$ M; $[HClO_4]$ = 0.05 M. The absorption with a maximum peak at approximately 400 nm is assumed as the product spectrum of the oxidation reaction. The molar absorptivity, ε, is calculated based on the stoichiometry that 1 equiv of biphenoquinone product is obtained from 2 equiv of Ir^{IV}.

$\varepsilon_{-OArArO^-} = 8.8 \times 10^3$ M^{-1} cm^{-1}, and $\varepsilon_{HOArArOH} = 4.9 \times 10^2$ M^{-1} cm^{-1}. The agreement between the pK_a values at these two wavelengths is excellent.

The two pK_a values for 2,2′-biphenol are quite different from those of the 4,4′ and 2,4′ isomers.[27] This difference is attributed to hydrogen bonding between the two O atoms, which is only possible for the 2,2′ isomer. The pK_{a1} values for all four coupling isomers are summarized in Table 1.

Overoxidation of Phenol. As shown below, Ir^{IV} oxidizes all four of these coupling isomers rapidly, which leads to overoxidation in the phenol reaction. A full account of the phenol reaction is thus dependent on the details of each of these overoxidation pathways.

1. Oxidation of 4,4′-Biphenol. Qualitatively, the reaction of Ir^{IV} with 4,4′-biphenol is signaled by the rapid loss of absorbance at 488 nm, which is characteristic of Ir^{IV}. A concurrent absorbance increase occurs at 398 nm, and this absorbance decays at longer time scales. A UV−vis spectrum of the 398 nm intermediate generated from the reaction of 2.5×10^{-5} M 4,4′-biphenol with 2.5×10^{-5} M Ir^{IV} at $p[H^+]$ = 5.5 is shown in Figure 8. This absorbance decays with an initial rate of -1.7×10^{-4} s^{-1}, as shown in Figure S-5 in the Supporting Information. When the same experiment is performed at $p[H^+]$ = 2.5, the maximum absorbance at 398 nm and its initial decay rate are close to those obtained at $p[H^+]$ = 5.5, as shown in Table S-7 in the Supporting Information. The species absorbing at 398 nm is assigned as 4,4′-biphenoquinone, which was claimed to be observed at 400 nm in the oxidation of phenol by other metal complexes.[29,30] Our results imply that the decomposition of 4,4′-biphenoquinone is almost pH-independent. The initial (maximum) absorbance of 4,4′-biphenoquinone at 398 nm yields a molar absorptivity 5.2×10^4 M^{-1} cm^{-1} in an aqueous solution, based on the assumption that 1 mol is produced per 2 mol of Ir^{IV}; this value for ε_{398} is consistent with the reported value ($\approx 5 \times 10^4$ M^{-1} cm^{-1}).[31]

In a spectrophotometric titration at $p[H^+]$ = 5.5, 4.8×10^{-5} M Ir^{IV} was added to 1.5 mL of 4.8×10^{-5} M 4,4′-biphenol, generating the titration curves in Figure S-6 in the Supporting Information. At 398 nm, the absorbance (after correction for dilution) rises linearly to an abrupt end point, and after the end point, the absorbance is stable. The end point corresponds to a consumption ratio of $n_{Ir^{IV}}/n_{4,4'\text{-biphenol}}$ of 2.5:1. Apparently, the 4,4′-biphenoquinone product undergoes some further overoxidation in the presence of 4,4′-biphenol. The absorbance at 488 nm (due to Ir^{IV}) remains essentially zero (Figure S-6b in the Supporting Information) prior to the same abrupt end point observed at 398 nm, implying that Ir^{IV} is fully consumed up to the end point.

The principal reaction is thus

$$2[IrCl_6]^{2-} + 4,4'\text{-biphenol} \rightarrow 2[IrCl_6]^{3-} + 4,4'\text{-biphenoquinone} + 2H^+ \quad (5)$$

Kinetic studies were performed with an excess of 4,4′-biphenol over Ir^{IV}, but because of its low solubility, the initial concentrations of 4,4′-biphenol were not high enough to ensure strictly pseudo-first-order conditions. Thus, values of k_{obs} were obtained from the slope of the linear regression of the logarithm of absorbance at 488 nm within the first half-life (Figure S-7 in the Supporting Information). Rates were determined at $p[H^+]$ = 1−7, and the data are shown in Table S-8 in the Supporting Information. These pH-dependent data conform to eq 2 (Figure 9), and they yield the

Table 1. Kinetic Data for the Reactions of Ir^{IV} with Phenol and Its Coupling Products[a]

substrate	k_{ArOH}, M^{-1} s^{-1}	k_{ArO^-}, M^{-1} s^{-1}	pK_{a1}	$E_f(ArO^•/ArO^-)$, V	$E_f(ArO^•,H^+/ArOH)$, V
phenol	0.77 ± 0.03	$(8.0 \pm 0.2) \times 10^6$	9.79[b]	0.80[f]	1.38
4,4′-biphenol	$(4.6 \pm 0.4) \times 10^4$	$(6.5 \pm 0.7) \times 10^8$	9.66[c]	0.64[d]	1.21
2,2′-biphenol	6.6 ± 2.6	$(4.0 \pm 0.7) \times 10^6$	7.60[d]	1.00[d]	1.45
2,4′-biphenol	$(4.0 \pm 0.6) \times 10^3$	$(1.3 \pm 0.3) \times 10^8$	9.67[c]		
4-phenoxyphenol	$(1.2 \pm 0.1) \times 10^3$	$(1.1 \pm 0.2) \times 10^8$	9.90[e]		

[a] Ar = 4,4′-/2,2′-/2,4′-$HOC_6H_4C_6H_4$, 4-$C_6H_5OC_6H_4$. Rate constants otained by fitting the k_{obs} results in Table S-8 in the Supporting Information to eq 2 and with the K_a values constrained to the values given above. [b] Reference 22. [c] This work. [d] Reference 27. [e] The reported pK_{a1} = 9.81 at μ = 0.25 M in ref [44] is converted to pK_{a1} = 9.90 at μ = 0.1 M by using the Davies equation. [f] E_f corrected in this work from $E°$ in ref 35.

dx.doi.org/10.1021/ic201897m | Inorg. Chem. 2011, 50, 12762–12773

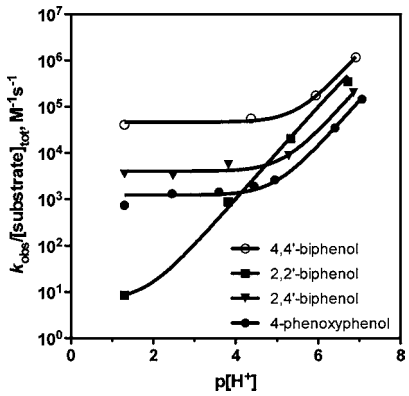

Figure 9. Plot of $k_{obs}/[substrate]_{tot}$ versus p[H$^+$]. $[Ir^{IV}]_0 = 2.5 \times 10^{-5}$ M; μ = 0.1 M ($LiClO_4$); T = 25 °C. At the p[H$^+$] values between 1.0 and 2.2, p[H$^+$] = −log [$HClO_4$]; the p[H$^+$] values between 2.4 and 3.6 were maintained by a 0.02 M monochloroacetate buffer; the p[H$^+$] values between 3.7 and 5.4 were maintained by a 0.02 M acetate buffer; the p[H$^+$] values between 5.5 and 7.1 were maintained by a 0.02 M cacodylate buffer. The solid lines are fits to eq 2.

following rate constants: $k_{ArOH} = (4.6 \pm 0.4) \times 10^4$ M^{-1} s^{-1} and $k_{ArO^-} = (6.5 \pm 0.7) \times 10^8$ M^{-1} s^{-1} (Table 1).

2. Oxidation of 2,2′-Biphenol. UV−vis spectroscopy was used to detect the products of the reaction between 1×10^{-3} M 2,2′-biphenol and 2.5×10^{-5} M Ir^{IV} at p[H$^+$] = 4.0. As shown in Figure 8, a weak absorbance peak appears at 406 nm with a broad shoulder observed in the range 450−600 nm. This spectrum is attributed to the absorption of 2,2′-biphenoquinone, with $\varepsilon_{406} = 1.4 \times 10^4$ M^{-1} cm^{-1} in an aqueous solution. It decomposes slowly as shown in Figure S-8 in the Supporting Information.

The kinetic experiments on the oxidation of 2,2′-biphenol by Ir^{IV} were performed by using stopped-flow spectroscopy to monitor the loss of Ir^{IV} at 488 nm at p[H$^+$] = 1−7 with at least a 10-fold molar excess of biphenol over Ir^{IV}. However, because of the absorbance of products at 488 nm and their subsequent decay, deviations from pseudo-first-order kinetics were observed at some p[H$^+$]. Therefore, the initial rate constants were calculated from the slopes of semilog plots of $(A - A_\infty)$ vs t. The reaction rates increase dramatically as the p[H$^+$] increases, although the oxidation is extremely slow at low p[H$^+$], as shown in Figure 9. Values for k_{ArOH} and k_{ArO^-} obtained by fitting the data in Table S-8 in the Supporting Information to eq 2 are 6.6 ± 3 and $(4.0 \pm 0.7) \times 10^6$ M^{-1} s^{-1}, respectively.

3. Oxidation of 2,4′-Biphenol. The products of the reaction between 2×10^{-4} M 2,4′-biphenol and 2.5×10^{-5} M Ir^{IV} at $[HClO_4]$ = 0.05 M were investigated by UV−vis spectroscopy. As shown in Figure S-9 in the Supporting Information, an intermediate that has an absorbance maximum at 398 nm is produced rapidly, and then it undergoes decomposition with a first-order rate constant of 7.2×10^{-3} s^{-1} (3.5×10^{-2} s^{-1} was obtained by a stopped-flow instrument at 488 nm, as shown in Table S-8 in the Supporting Information). The first UV−vis spectrum obtained after mixing (~10 s) is shown in Figure 8; it has a main peak at 398 nm and a minor peak at 488 nm (overlapping with that of Ir^{IV}). Assignment of this spectrum to 2,4′-biphenoquinone is supported by density functional theory calculations at the B3LYP/6-31G* level that produce an electronic spectrum with a major peak at ~320 nm and a secondary peak at 460 nm. With the assumption of a 2:1 Ir^{IV}/2,4′-biphenoquinone stoichiometry, the experimental spectrum yields $\varepsilon_{398} = 3.0 \times 10^4$ M^{-1} cm^{-1} and $\varepsilon_{488} = 4.0 \times 10^3$ M^{-1} cm^{-1}.

At p[H$^+$] = 6.9 and 398 nm, the kinetic traces are triphasic, showing a rapid rise in absorbance, a slower small-amplitude fall, and then an even slower large-amplitude fall (Figure S-10 in the Supporting Information). The first phase occurs on the same time frame as the initial absorbance loss at 488 nm (see below). This triphasic behavior is thus attributed to the rapid production of 2,4′-biphenoquinone in the first phase, followed by its biphasic decay. Because of the relatively rapid decay in the second phase, it was not possible to obtain an accurate value for ε_{398} at this pH, a value of only 1.6×10^4 M^{-1} cm^{-1} corresponding to the maximum absorbance.

At 488 nm, the kinetic traces exhibit biphasic decay. Double-exponential fits were used to obtain the fast pseudo-first-order rate constants for the consumption of Ir^{IV} (k_{obs}) as well as the slower first-order rate constants for the decay of 2,4′-biphenoquinone ($k_{obs,2}$) (shown in Table S-8 in the Supporting Information). The p[H$^+$] dependence of the Ir^{IV} reduction was studied at p[H$^+$] = 1−7. A fit of the values of k_{obs} to eq 2 generated $k_{ArOH} = (4.0 \pm 0.6) \times 10^3$ M^{-1} s^{-1} and $k_{ArO^-} = (1.3 \pm 0.3) \times 10^8$ M^{-1} s^{-1} (Table 1).

4. Oxidation of 4-Phenoxyphenol. Kinetic studies of the reaction of 0.3 mM 4-phenoxyphenol with 25 μM Ir^{IV} were carried out in the range p[H$^+$] = 1−7. The decay traces of Ir^{IV} at 488 nm display excellent pseudo-first-order behavior under these conditions (Table S-8 in the Supporting Information). A fit of the data to rate law (2) led to the following parameters: $k_{ArOH} = (1.2 \pm 0.1) \times 10^3$ M^{-1} s^{-1} and $k_{ArO^-} = (1.1 \pm 0.2) \times 10^8$ M^{-1} s^{-1} (Table 1).

Evidence of Overoxidation of Phenol. As shown in Figure 10, the reaction between 0.0443 M phenol and 1×10^{-4} M Ir^{IV} at p[H$^+$] = 2.5 displays a loss of absorbance at 488 nm, signaling the consumption of Ir^{IV}, and there is a concurrent rise in absorbance at 398 nm that is assigned to the formation of biphenoquinones arising from oxidation of the biphenol coupling products. Figure S-11 in the Supporting Information displays the absorbance at 398 nm on a longer time scale to demonstrate the rise−fall character of the signal. A double-exponential nonlinear regression fit generates two observed rate constants: the fast one is 3.6×10^{-2} s^{-1}, and it corresponds to

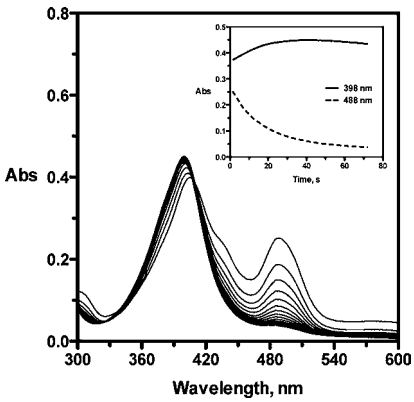

Figure 10. UV−vis spectra of the reaction between 4.43×10^{-2} M phenol and 1×10^{-4} M Ir^{IV}. p[H$^+$] = 2.5 (0.02 M monochloroacetate buffer); μ = 0.1 M ($LiClO_4$); T = 25 °C; 5 s interval between spectra. The inset shows the kinetic traces at 398 nm (solid line) and 488 nm (dashed line).

dx.doi.org/10.1021/ic201897m | Inorg. Chem. 2011, 50, 12762−12773

the consumption of Ir^{IV} at 488 nm, while the slow one is 3.7×10^{-3} s^{-1}, which corresponds to the decay of 2,4′-biphenoquinone (Table S-7 in the Supporting Information).

DISCUSSION

The initial steps in the oxidation of phenol by Ir^{IV} are now well established.[2,5] First, depending on the pH, either phenol itself or its conjugate base undergoes reversible one-electron oxidation to produce the phenoxyl radical and $[IrCl_6]^{3-}$. Next, the phenoxyl radicals undergo bimolecular C−C coupling to produce biphenols and C−O coupling to produce phenoxyphenol. Crucial evidence for this mechanism includes the pH dependence of the rates, the kinetic inhibition by Ir^{III} and its removal by the spin-trap DBNBS, and the simulation of these effects with a kinetic model employing realistic values for the four redox rate constants and the radical coupling overall rate constant. Early on, Cecil and Littler recognized that this model is incomplete because it fails to account for the observed production of diphenoquinone;[2] they proposed that the initial diphenol coupling products were oxidized further, generating diphenoquinone. Our in situ UV−vis data provide further evidence for this overoxidation mechanism. Our current studies of the direct oxidations of the four principal phenoxyl coupling products allow quantitative tests of the overoxidation mechanism, and they provide an explanation of the apparent pH-dependent rate constant (k° in eq 3).

As shown in Figure 9, all four coupling products are oxidized by Ir^{IV} with rates that are highly sensitive to the pH. Moreover, they all (and phenol itself) have two-term rate laws, as given by eq 2. A notable difference between the oxidations of the biphenols and phenol is that the biphenols undergo net two-electron oxidation to yield quinones, while phenol undergoes net one-electron oxidation to yield radical coupling products. Evidently, the biphenols achieve their two-electron oxidations through one-electron oxidation of the biphenols and their conjugate bases to form semiquinones, followed by the rapid one-electron conversion of the semiquinones to the quinones. Radical coupling occurs in the case of phenol because the phenoxyl radical is not easily oxidized to its cation.

The overall oxidation of 4,4′-biphenol by Ir^{IV}, as in eq 5, is close to thermoneutral at pH = 1 because E°(4,4′-biphenoquinone,$2H^+$/4,4′-biphenol) = 0.94 V vs NHE[32] while $E^\circ(Ir^{IV}/Ir^{III})$ = 0.893 V.[33] This reaction becomes more favorable as the pH increases. In view of the overall stoichiometry (eq 5) and the two-term rate law (eq 2), a reasonable reaction mechanism is

$$4,4'\text{-}HOC_6H_4C_6H_4OH \rightleftarrows 4,4'\text{-}HOC_6H_4C_6H_4O^- + H^+ \qquad K_a \tag{6}$$

$$Ir^{IV} + 4,4'\text{-}HOC_6H_4C_6H_4OH \rightleftarrows Ir^{III} + 4,4'\text{-}HOC_6H_4C_6H_4O^\bullet + H^+ \qquad K_{ArOH},\ k_{ArOH},\ k_{-ArOH} \tag{7}$$

$$Ir^{IV} + 4,4'\text{-}HOC_6H_4C_6H_4O^- \rightleftarrows Ir^{III} + 4,4'\text{-}HOC_6H_4C_6H_4O^\bullet \qquad K_{ArO^-},\ k_{ArO^-},\ k_{-ArO^-} \tag{8}$$

$$2[4,4'\text{-}HOC_6H_4C_6H_4O^\bullet] \rightarrow 4,4'\text{-biphenol} + 4,4'\text{-biphenoquinone} \qquad k_{disp,4,4} \tag{9}$$

$$Ir^{IV} + 4,4'\text{-}HOC_6H_4C_6H_4O^\bullet \rightarrow Ir^{III} + 4,4'\text{-biphenoquinone} + H^+ \qquad k_{semi} \tag{10}$$

Here, direct oxidation of the biphenol generates the biphenosemiquinone through a concerted electron−proton-transfer mechanism. This step is uphill and, hence, is shown as reversible because E°(4,4′-$HOC_6H_4C_6H_4O^\bullet$,H^+/4,4′-$HOC_6H_4C_6H_4OH$) is 1.21 V [calculated from $E^\circ(ArO^\bullet,H^+/ArOH) = E^\circ(ArO^\bullet/ArO^-) + 0.059pK_a$ with $E^\circ(ArO^\bullet/ArO^-)$ = 0.64 V vs NHE[27]]. Oxidation of the conjugate base of biphenol occurs through simple electron transfer; both of these are in direct analogy with the oxidation of phenol. The fate of the semiquinone could be either disproportionation, as in eq 9, or further oxidation, as in eq 10. Disproportionation was reported previously for the semiquinone in the absence of good oxidants;[30] although the disporportionation rate constant was not determined, it can be expected to be large because the reaction has a large driving force: E°(4,4′-biphenoquinone,$2H^+$/4,4′-biphenol) = 0.94 V vs NHE[32] and E°(4,4′-$HOC_6H_4C_6H_4O^\bullet$,H^+/4,4′-$HOC_6H_4C_6H_4OH$) = 1.21 V vs NHE. On the other hand, semiquinones are easily oxidized,[34] and the oxidation of 4,4′-biphenosemiquinone is quite favorable: E°(4,4′-biphenoquinone,H^+/4,4′-biphenosemiquinone) = 0.67 V (as calculated from the above data). Moreover, the semiquinone is relatively acidic with a pK_a of 4,4′-$HOC_6H_4C_6H_4O^\bullet$ of 6.3.[27] Clearly, a large rate constant can be anticipated for k_{semi}. The low steady-state concentration of the semiquinone ensures that its reaction with Ir^{IV} will be dominant.

2,2′-Biphenol is more acidic than 4,4′-biphenol by about 2 pK units. This difference is attributed to the formation of an internal hydrogen bond between the two O atoms in the 2,2′-biphenolate monoanion. The value of k_{ArO^-} is about a factor of 100 less for 2,2′-biphenol than for 4,4′-biphenol (for reasons discussed below). The result of these two effects is that the rates of oxidation of the two biphenol isomers are quite similar at pH = 7. On the other hand, the value for k_{ArOH} is 10 000-fold less for 2,2′-biphenol, so the pH-independent region of the rate law is limited to only quite acidic conditions (Figure 9). Despite these quantitative differences, we infer the same qualitative mechanism for oxidation of the two substrates.

Unlike 2,2′-biphenol, 2,4′-biphenol is incapable of internal hydrogen bonding and thus resembles 4,4′-biphenol quite closely in its oxidation by Ir^{IV}.

4-Phenoxyphenol has a pK_a value and values for k_{ArOH} and k_{ArO^-} that are similar to those of 4,4′-biphenol, and hence its rate−pH profile is similar. Upon oxidation, it yields the 4-phenoxyphenoxyl radical rather than a semiquinone, and hence the ultimate product is due to radical coupling.

The above considerations lead to the following mechanism for the overall oxidation of phenol:

dx.doi.org/10.1021/ic201897m | Inorg. Chem. 2011, 50, 12762–12773

$$Ir^{IV} + C_6H_5OH \rightleftarrows Ir^{III} + C_6H_5O^{\bullet} + H^+ \quad K_{ArOH},\ k_{ArOH},\ k_{-ArOH} \tag{11}$$

$$Ir^{IV} + C_6H_5O^- \rightleftarrows Ir^{III} + C_6H_5O^{\bullet} \quad K_{ArO^-},\ k_{ArO^-},\ k_{-ArO^-} \tag{12}$$

$$C_6H_5OH \rightleftarrows C_6H_5O^- + H^+ \quad K_a \tag{13}$$

$$2C_6H_5O^{\bullet} \rightarrow 4,4'\text{-biphenol} \quad k_{dim,4,4} \tag{14a}$$

$$2C_6H_5O^{\bullet} \rightarrow 2,2'\text{-biphenol} \quad k_{dim,2,2} \tag{14b}$$

$$2C_6H_5O^{\bullet} \rightarrow 2,4'\text{-biphenol} \quad k_{dim,2,4} \tag{14c}$$

$$2C_6H_5O^{\bullet} \rightarrow 4\text{-phenoxyphenol} \quad k_{dim,pop} \tag{14d}$$

$$Ir^{IV} + 4,4'\text{-biphenol} \rightarrow Ir^{III} + 4,4'\text{-}HOC_6H_4C_6H_4O^{\bullet} + H^+ \quad k_{overox1,4,4} \tag{15a}$$

$$Ir^{IV} + 2,2'\text{-biphenol} \rightarrow Ir^{III} + 2,2'\text{-}HOC_6H_4C_6H_4O^{\bullet} + H^+ \quad k_{overox1,2,2} \tag{15b}$$

$$Ir^{IV} + 2,4'\text{-biphenol} \rightarrow Ir^{III} + 2,4'\text{-}HOC_6H_4C_6H_4O^{\bullet} + H^+ \quad k_{overox1,2,4} \tag{15c}$$

$$Ir^{IV} + 4'\text{-phenoxyphenol} \rightarrow Ir^{III} + 4\text{-}C_6H_5OC_6H_4O^{\bullet} + H^+ \quad k_{overox1,pop} \tag{15d}$$

$$Ir^{IV} + 4,4'\text{-}HOC_6H_4C_6H_4O^{\bullet} \rightarrow Ir^{III} + 4,4'\text{-biphenoquinone} + H^+ \quad k_{overox2,4,4} \tag{16a}$$

$$Ir^{IV} + 2,2'\text{-}HOC_6H_4C_6H_4O^{\bullet} \rightarrow Ir^{III} + 2,2'\text{-biphenoquinone} + H^+ \quad k_{overox2,2,2} \tag{16b}$$

$$Ir^{IV} + 2,4'\text{-}HOC_6H_4C_6H_4O^{\bullet} \rightarrow Ir^{III} + 2,4'\text{-biphenoquinone} + H^+ \quad k_{overox2,2,4} \tag{16c}$$

$$2[4\text{-}C_6H_5OC_6H_4O^{\bullet}] \rightarrow 4\text{-products} \quad k_{dec,pop} \tag{16d}$$

The first step in this mechanism corresponds to the reversible concerted proton-electron-transfer oxidation of neutral phenol, and the second step is the reversible outer-sphere electron transfer from the phenolate anion. The acid/base reaction relating phenol and phenolate (eq 13) is assumed to be at equilibrium because of rapid proton transfer. Values for k_{ArOH} and k_{ArO^-} are directly measured as described above, while values for k_{-ArOH} and k_{-ArO^-} are calculated from the forward rate constants and the E_f values at μ = 0.1 M: $E_f(Ir^{IV}/Ir^{III})$ = 0.893 V,[33] $E_f(C_6H_5O^{\bullet}/C_6H_5O^-)$ = 0.80 V, corrected from 0.79 V at μ = 0.0 M[35] by log $\gamma = -Az_i^2\mu^{1/2}/(1 + \mu^{1/2})$, and $E_f(C_6H_5O^{\bullet},H^+/C_6H_5OH)$ = 1.38 V [calculated from $E_f(ArO^{\bullet},H^+/ArOH) = E_f(ArO^{\bullet}/ArO^-) + 0.059pK_a$]. Dimerization of the phenoxyl radical, which can be partially rate-limiting under certain conditions, forms the four major coupling isomers: 4,4′-, 2,2′-, and 2,4′-biphenol and 4-phenoxyphenol. Under the assumption that the dimerization rate constant producing each species is proportional to its yield, $k_{dim,4,4}$, $k_{dim,2,2}$, $k_{dim,2,4}$, and $k_{dim,pop}$ in eqs 14a–14d are 2.88×10^8, 2.07×10^8, 5.06×10^8, and 1.04×10^8 M^{-1} s^{-1}, respectively, according to the reported overall $2k_{dim}$ value[36] and yield of each isomer.[25]

Further one-electron oxidations of the phenol coupling products are shown in eqs 15a–15d without reference to the pH dependence evident in Figure 9. In our simulations described below, the rate constants for these steps, $k_{overox1,4,4}$, $k_{overox1,2,2}$, $k_{overox1,2,4}$, and $k_{overox1,pop}$, are conditional on the pH and are derived from the parameters in Table 1. Equations 16a–16d depict the semiquinones as undergoing oxidation by Ir^{IV}; in the simulations, we assign rapid rate constants for these oxidations, but the results are insensitive to the exact values used. Equation 16d depicts a rapid second-order decay through dimerization for the phenoxyphenoxyl radical based on analogy with other phenoxyl radicals.

Kinetic simulations of the oxidation of phenol based on the above mechanism were performed by use of the *Specfit/32* computer program,[37] with the exact model as specified in Table S-9 in the Supporting Information. These simulations yielded decays of $[Ir^{IV}]$, the half-lives of which were then used to generate simulated pseudo-first-order rate constants, $k_{obs,sim}$. Figure 11a (data from Table S-11 in the Supporting Information) shows that these results give an excellent fit to the experimental pH dependence of the reaction. Figure 11b compares the simulated results from the full mechanism with

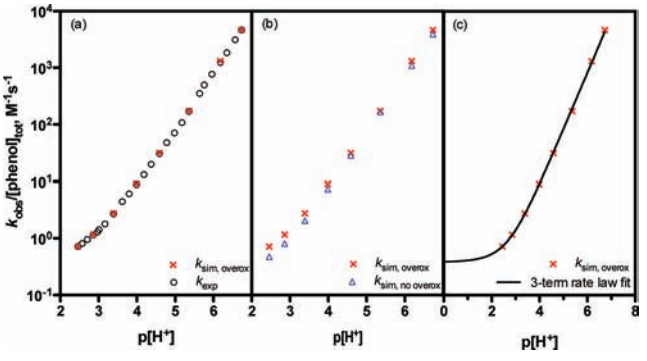

Figure 11. Comparative pH dependence of the phenol reaction experimental data and simulation results: (a) experimental data and simulated results with overoxidation; (b) simulated results with and without overoxidation; (c) simulated results with overoxidation and its three-term rate law curve fit.

dx.doi.org/10.1021/ic201897m | *Inorg. Chem.* 2011, 50, 12762–12773

those obtained when overoxidation (eqs 15a−15d and 16a−16d) is excluded from the mechanism, and it shows that overoxidation increases the net rates at low pH but less so at higher pH. As a result, overoxidation leads to a pH dependence that deviates systematically from the simple two-term rate law in eq 2. Figure 11c shows that the simulations with overoxidation included give an excellent fit to the three-term rate law (eq 3), with fitted values of $k_{ArOH} = 0.38 \pm 0.14$ M^{-1} s^{-1}, $k_{ArO^-} = (4.9 \pm 0.2) \times 10^6$ M^{-1} s^{-1}, and $k^\circ = (8.2 \pm 7) \times 10^{-3}$ M^{-1} s^{-1}. Although the statistical uncertainty in k° is large, the value of k° is in good agreement with the value derived from the experimental data. Evidently, the origin of the k° term in the fit of the empirical rate law (3) to the experimental results is the pH-dependent influence of overoxidation on the rate of consumption of Ir^{IV}.

If overoxidation were not occurring, the rate constants in eq 2 would agree exactly with those in the mechanism, corresponding to a stoichiometric factor of unity in the rate law. An effect of overoxidation is that the rate constants derived from eq 2 are somewhat larger than the rate constants for the elementary steps, which means that overoxidation introduces stoichiometric factors greater than unity. These stoichiometric factors, calculated as the ratio k_{sim}(with overoxidation)/k_{sim}(without overoxidation), decrease systematically from 1.75 at pH 2.46 to 1.10 at pH 5.36 (Table S-11 in the Supporting Information). They also depend somewhat on the phenol concentration. It is the pH dependence of the stoichiometric factor that leads to the k° term in rate law (3).

Another consequence of the pH-dependent stoichiometric factor is that the yields of the reaction products are also pH-dependent. As shown in Table S-12 in the Supporting Information, at pH 2.46 the simulated yield of the initial coupling products per 1 mol of Ir^{IV} (corrected for the 1:2 stoichiometric ratio) is 9.6% and the yield of the overoxidation products (corrected for the 1:4 stoichiometric ratio) is 90.4%. However, at pH 5.36 these yields cross over to 72.9% and 27.1%, respectively.

In the presence of the spin-trap DBNBS, three more steps are added to the above mechanism:

$$(DBNBS)_2 \rightleftarrows 2DBNBS \qquad K_{dim,DBNBS},\ k_{dim,DBNBS},\ k_{-dim,DBNBS} \tag{17}$$

$$C_6H_5O^\bullet + DBNBS \rightarrow adduct^\bullet \qquad k_{DBNBS} \tag{18}$$

$$Ir^{IV} + adduct^\bullet \rightarrow Ir^{III} + adduct^+ \qquad k_{adduct} \tag{19}$$

As mentioned above, only the monomer of DBNBS can scavenge the phenoxyl radical. Therefore, the dimerization step of DBNBS with equilibrium constant $K_{dim,DBNBS}$ of 1.3×10^{-3} M should be included in our mechanism.[21] The phenoxyl radical is scavenged by DBNBS to form an adduct, which undergoes a rapid oxidation by Ir^{IV}, as in eqs 18 and 19. Competition between the scavenging of the phenoxyl radical by DBNBS and its dimerization is evident in the kinetic saturation dependence on [DBNBS], as shown in Table S-2 in the Supporting Information. Simulations of this saturation effect at p[H^+] = 1.3, performed with the mechanism in Table S-9 in the Supporting Information, are sensitive to the value of k_{DBNBS}. As shown in Table S-13 in the Supporting Information, a good fit is obtained when the rate constant of $C_6H_5O^\bullet$/DBNBS adduct formation, k_{DBNBS}, is 2.0×10^5 M^{-1} s^{-1}. This rate constant is large enough to enable 10 mM concentrations of DBNBS to scavenge the phenoxyl radicals completely, preventing their back-reaction with Ir^{III} and ensuring that the rate-limiting step in the oxidation by Ir^{IV} is the initial oxidation of phenol.

A remaining question is the origin of the pH dependence of the $[Ru(bpy)_3]^{3+}$/phenol reaction reported by Sjödin et al., which required the three-term eq 3.[6] First, we note that Bonin et al. were unable to reproduce the effect and found the two-term eq 2 to be adequate.[3] Second, the degree of overoxidation to be expected depends on the phenol concentration, and this concentration was not disclosed in the original report. Third, the degree of overoxidation should also depend on the rate constants for $[Ru(bpy)_3]^{3+}$ oxidation of the phenolic coupling products, and these rate constants are unknown. However, it can be shown that a significant degree of overoxidation should occur in acidic media if favorable choices are made for the reactant concentrations and rate constants.

Rate Constant Trends. Table 1 shows that the values for k_{ArO^-} range from 4×10^6 to 6.5×10^8 M^{-1} s^{-1} for the five phenolate ions considered in this study. These rate constants correspond to electron-transfer reactions, and hence it is reasonable to use the cross-relationship of Marcus theory, as given in eqs 20−23, to rationalize their variations.[38]

$$k_{12} = (k_{11}k_{22}K_{12}f_{12})^{1/2}W_{12} \tag{20}$$

$$\ln f_{12} = \frac{[\ln K_{12} + (w_{12} - w_{21})/RT]^2}{4[\ln(k_{11}k_{22}/Z^2) + (w_{11} + w_{22})/RT]} \tag{21}$$

$$W_{12} = \exp[(-w_{12} - w_{21} + w_{11} + w_{22})/2RT] \tag{22}$$

$$w_{ij} = 17.1Z_iZ_j/r(1 + 0.328r\mu^{1/2}) \tag{23}$$

In these equations, k_{12} is the cross-electron-transfer rate constant ($k_{ArO^-} = 8.0 \times 10^6$ M^{-1} s^{-1} for phenoxide), and k_{11} and k_{22} are the self-exchange rate constants of the $ArO^\bullet/ArO^-$ and Ir^{IV}/Ir^{III} redox couples, respectively. A value for k_{22} of 2×10^5 M^{-1} s^{-1} is used in the calculation,[39] and 1×10^{11} M^{-1} s^{-1} is used for Z, the collision frequency.[40] Z_i and Z_j are ionic charges of the reactants, R is the ideal gas constant, and r is the center-to-center distance between the two reactants when they are approaching each other. The radii of $[IrCl_6]^{2-}$ and $C_6H_5O^-$ are 4.1[41] and 2.5 Å, respectively, estimated from Corey−Pauling−Koltun atomic models. μ is the ionic strength. w_{ij} is the electrostatic energy between reactants i and j. If the distance r is in angstroms and μ in molar, then w_{12} can be calculated according to eq 23 in kilojoules per mole. With all of these parameters and the experimental values of k_{12} and K_{12}, k_{11} is calculated from the above equations as 2.3×10^6 M^{-1} s^{-1}. The phenoxide anion and the phenoxyl radical are predicted to have quite similar structures, with the largest difference being a 0.015 Å change in the C−O bond length.[42] Such a small structural change should not contribute significantly to the self-exchange barrier. Estimates of the solvation contribution to the self-exchange barrier ($\Delta G_{os}^{\ddagger}$) are difficult to make because the phenolate charge is highly localized on the oxygen end of the anion; however, this charge localization should cause $\Delta G_{os}^{\ddagger}$ to be larger than that for a spherical anion of comparable size. As a result, the significant overall self-exchange barrier implied by the k_{11} above value is attributed principally to the solvent barrier. A significantly greater value for k_{11} of 1.9×10^8 M^{-1} s^{-1} was previously measured directly by electron spin resonance line broadening.[43] Apparently, the solvent barrier is reduced in

dx.doi.org/10.1021/ic201897m | Inorg. Chem. 2011, 50, 12762−12773

the actual self-exchange process, possibly through a weak association between the radical and the phenoxide anion.

In the case of the 4,4′-biphenoxide anion [$E°(ArO^{\bullet}/ArO^{-})$ = 0.64 V],[27] k_{ArO^-} is considerably larger than that for phenoxide itself. Most of this increase can be ascribed to the greater driving force for the reaction, but there is also some contribution from a greater self-exchange rate constant (k_{11} = 4×10^7 M^{-1} s^{-1}). A reduced self-exchange barrier can be attributed to the delocalized electronic structure of the semiquinone radical.

The 2,2′-biphenoxide anion is considerably more difficult to oxidize [$E°(ArO^{\bullet}/ArO^{-})$ = 1.00 V][27] than phenoxide, but the two substrates have quite similar k_{ArO^-} values. A large self-exchange rate constant of 3×10^8 M^{-1} s^{-1} is required by these data. It is conceivable that the internal hydrogen bonding in the 2,2′ isomer reduces the degree of hydrogen bonding with the solvent and thus leads to a greater k_{11} value. Corresponding discussions of the 2,4′-biphenoxide and 4-phenoxyphenoxide rates will require determination of the relevant $E°$ values.

We have previously argued that the direct oxidation of phenol by Ir^{IV} (eq 11, k_{ArOH}) involves proton transfer to the solvent in concert with electron transfer (H_2O-PCET).[5] This mechanistic assignment was based largely on the significant solvent deuterium KIE, the high acidity of the $ArOH^{\bullet+}$ radical cation, and the low basicity of Ir^{III}. This conclusion is strengthened by the CV measurements described above, which show that Ir^{III} is not significantly protonated in 1 M H^+. Further support for this H_2O-PCET mechanism is provided by a linear free-energy relationship that relates the rates of oxidation of phenol to the $E°$ values for Ir^{IV} and a set of three Ru^{III} oxidants.[3] It seems reasonable to assign a H_2O-PCET mechanism to all of the phenol reactions in Table 1. Recently, Bonin et al. have developed a theoretical treatment of CPET reactions with water (and other bases) as the proton acceptor;[4] this theory predicts, in the absence of other effects, that these reactions should display a typically Marcusian dependence of the rates on the driving forces. Qualitatively, Table 1 shows that this expectation is met in comparing phenol with 4,4′-biphenol and in comparing 4,4′-biphenol with 2,2′-biphenol. However, 2,2′-biphenol reacts 9 times faster than phenol, even though it is 0.07 V more difficult to oxidize. This apparent contradiction may signal the importance of several other variables in the theory of H_2O-PCET.

■ ASSOCIATED CONTENT

Ⓢ Supporting Information

Thirteen tables of kinetic data, four figures of spectra, six figures of kinetic data, and one figure of spectrophotometric titration data. This material is available free of charge via the Internet at http://pubs.acs.org.

■ AUTHOR INFORMATION

Corresponding Author

*E-mail: stanbury@auburn.edu.

■ ACKNOWLEDGMENTS

We thank the NSF for support of this research.

■ REFERENCES

(1) Huynh, M. H. V.; Meyer, T. J. *Chem. Rev.* **2007**, *107*, 5004−5064.
(2) Cecil, R.; Littler, J. S. *J. Chem. Soc. B* **1968**, 1420−1427.
(3) Bonin, J.; Costentin, C.; Louault, C.; Robert, M.; Routier, M.; Savéant, J.-M. *Proc. Natl. Acad. Sci. U.S.A.* **2010**, *107*, 3367−3372.
(4) Bonin, J.; Costentin, C.; Louault, C.; Robert, M.; Saveant, J. M. *J. Am. Chem. Soc.* **2011**, *133*, 6668−6674.
(5) Song, N.; Stanbury, D. M. *Inorg. Chem.* **2008**, *47*, 11458−11460.
(6) Sjödin, M.; Irebo, T.; Utas, J. E.; Lind, J.; Merényi, G.; Åkermark, B.; Hammarström, L. *J. Am. Chem. Soc.* **2006**, *128*, 13076−13083.
(7) Kauffman, G. B.; Teter, L. A. *Inorg. Synth.* **1966**, *8*, 223−227.
(8) Perrin, D. D.; Armarego, W. L. F. *Purification of Laboratory Chemicals*, 3rd ed.; Pergamon: New York, 1988.
(9) Kaur, H.; Leung, K. H. W.; Perkins, M. J. *J. Chem. Soc., Chem. Commun.* **1981**, 142−143.
(10) Hamilton, L.; Nielsen, B. R.; Davies, C. A.; Symons, M. C. R.; Winyard, P. G. *Free Radical Res.* **2003**, *37*, 41−49.
(11) Kanetani, F.; Yamaguchi, H. *Bull. Chem. Soc. Jpn.* **1981**, *54*, 3048−3058.
(12) Konaka, R.; Sakata, S. *Chem. Lett.* **1982**, 411−414.
(13) Amblard, F.; Govindarajan, B.; Lefkove, B.; Rapp, K. L.; Detorio, M.; Arbiser, J. L.; Schinazi, R. F. *Bioorg. Med. Chem. Lett.* **2007**, *17*, 4428−4431.
(14) Sarala, R.; Stanbury, D. M. *Inorg. Chem.* **1990**, *29*, 3456−3460.
(15) Sawyer, D. T.; Sobkowiak, A.; Roberts, J. L. *Electrochemistry for Chemists*, 2nd ed.; John Wiley and Sons: New York, 1995; p 192.
(16) *Spartan '08*; Wavefunction, Inc.: Irvine, CA, 2008.
(17) Bruhn, H.; Nigam, S.; Holzwarth, J. F. *Faraday Discuss. Chem. Soc.* **1982**, *74*, 129−140.
(18) Bonin, J.; Costentin, C.; Robert, M.; Saveant, J. M. *Org. Biomol. Chem.* **2011**, *9*, 4064−4069.
(19) Irebo, T.; Reece, S. Y.; Sjödin, M.; Nocera, D. G.; Hammarström, L. *J. Am. Chem. Soc.* **2007**, *129*, 15462−15464.
(20) Zalomaeva, O. V.; Trukhan, N. N.; Ivanchikova, I. D.; Panchenko, A. A.; Roduner, E.; Talsi, E. P.; Sorokin, A. B.; Rogov, V. A.; Khodeeva, O. A. *J. Mol. Catal. A* **2007**, *277*, 185−192.
(21) Ide, H.; Hagi, A.; Ohzumi, S.; Murakami, A.; Makino, K. *Biochem. Int.* **1992**, *27*, 367−372.
(22) Martell, A. E.; Smith, R. M.; Motekaitis, R. J. *NIST Critically Selected Stability Constants of Metal Complexes Database*, version 7.0; U.S. Department of Commerce: Gaithersburg, MD, 2003.
(23) Fine, D. A. *Inorg. Chem.* **1969**, *8*, 1014−1016.
(24) Makarycheva-Mikhailova, A. V.; Stanbury, D. M.; McKee, M. L. *J. Phys. Chem. B* **2007**, *111*, 6942−6948.
(25) Ye, M.; Schuler, R. H. *J. Phys. Chem.* **1989**, *93*, 1898−1902.
(26) Das, T. N. *J. Phys. Chem. A* **2001**, *105*, 5954−5959.
(27) Jonsson, M.; Lind, J.; Merényi, G. *J. Phys. Chem. A* **2002**, *106*, 4758−4762.
(28) Jonsson, M.; Lind, J.; Merényi, G. *J. Phys. Chem. A* **2003**, *107*, 5878−5879.
(29) Al-Ajlouni, A.; Bakac, A.; Espenson, J. H. *Inorg. Chem.* **1993**, *32*, 5792−5796.
(30) Papina, A. A.; Koppenol, W. H. *Chem. Res. Toxicol.* **2007**, *20*, 2021−2022.
(31) Al-Ajlouni, A. M.; Shawakfeh, K. Q.; Rajal, R. *Kinet. Catal.* **2009**, *50*, 88−96.
(32) Pelizzetti, E.; Mentasti, E. *J. Inorg. Nucl. Chem.* **1977**, *39*, 2227−2230.
(33) Margerum, D. W.; Chellappa, K. L.; Bossu, F. P.; Burce, G. L. *J. Am. Chem. Soc.* **1975**, *97*, 6894−6896.
(34) Neta, P.; Grodkowski, J. *J. Phys. Chem. Ref. Data* **2005**, *34*, 109−199.
(35) Lind, J.; Shen, X.; Eriksen, T. E.; Merényi, G. *J. Am. Chem. Soc.* **1990**, *112*, 479−482.
(36) Tripathi, G. N. R.; Schuler, R. H. *J. Chem. Phys.* **1982**, *88*, 253−255.
(37) Binstead, R. A.; Jung, B.; Zuberbuhler, A. D. *Specfit/32 Global Analysis System*, version 3.0; Spectrum Software Associates: Marlborough, MA, 2000.
(38) Zuckerman, J. J. *Inorganic Reactions and Methods*; VCH: Deerfield Beach, FL, 1986; Vol. *15*, pp 13−47.
(39) Hurwitz, P.; Kustin, K. *Trans. Faraday Soc.* **1966**, *62*, 427−432.
(40) Ram, M. S.; Stanbury, D. M. *J. Phys. Chem.* **1986**, *90*, 3691−3696.

(41) Sun, J.; Stanbury, D. M. *J. Chem. Soc., Dalton Trans.* **2002**, 785–791.
(42) McDonald, W. J.; Einarsdóttir, O. *J. Phys. Chem. A* **2008**, *112*, 11400–11413.
(43) Schuler, R. H.; Neta, P.; Zemel, H.; Fessenden, R. W. *J. Am. Chem. Soc.* **1976**, *98*, 3825–3831.
(44) Stradins, J.; Hasanli, B. *J. Electroanal. Chem.* **1993**, *353*, 57–69.